remote sensing

MDPI

Article

Estimation of Biomass and N Uptake in Different Winter Cover Crops from UAV-Based Multispectral Canopy Reflectance Data

Katja Holzhauser *, Thomas Räbiger, Till Rose, Henning Kage and Insa Kühling

Institute of Crop Science and Plant Breeding, Kiel University, 24118 Kiel, Germany
* Correspondence: holzhauser@pflanzenbau.uni-kiel.de

Abstract: Cover crops are known to provide beneficial effects to agricultural systems such as a reduction in nitrate leaching, erosion control, and an increase in soil organic matter. The monitoring of cover crops' growth (e.g., green area index (GAI), nitrogen (N) uptake, or dry matter (DM)) using remote sensing techniques allows us to identify the physiological processes involved and to optimise management decisions. Based on the data of a two-year trial (2018, 2019) in Kiel, Northern Germany, the multispectral sensor Sequoia (Parrot) was calibrated to the selected parameters of the winter cover crops oilseed radish, saia oat, spring vetch, and winter rye as sole cover crops and combined in mixtures. Two simple ratios (SR_{red}, $SR_{red\ edge}$) and two normalised difference indices (ND_{red}, $ND_{red\ edge}$) were calculated and tested for their predicting power. Furthermore, the advantage of the species/mixture–individual compared to the universal models was analysed. SR_{red} best predicted GAI, DM, and N uptake (R^2: 0.60, 0.53, 0.45, respectively) in a universal model approach. The canopy parameters of saia oat and spring vetch were estimated by species–individual models, achieving a higher R^2 than with the universal model. Comparing mixture–individual models to the universal model revealed low relative error differences below 3%. The findings of the current study serve as a tool for the rapid and inexpensive estimation of cover crops' canopy parameters that determine environmental services.

Keywords: remote sensing; Parrot Sequoia; catch crops; sensor calibration; pure and mixed canopies; NDVI

Citation: Holzhauser, K.; Räbiger, T.; Rose, T.; Kage, H.; Kühling, I. Estimation of Biomass and N Uptake in Different Winter Cover Crops from UAV-Based Multispectral Canopy Reflectance Data. *Remote Sens.* **2022**, *14*, 4525. https://doi.org/10.3390/rs14184525

Academic Editor: Mark J. Lara

Received: 3 August 2022
Accepted: 8 September 2022
Published: 10 September 2022

1. Introduction

Cover crops have gained importance during the last decade, as they provide ecosystem services such as a reduction in nitrate leaching, erosion control, and an increase in soil organic matter (SOM) [1–3]. Implementing incentives for growing winter cover crops within the common agricultural policy of the European union has encouraged their widespread cultivation [4]. Closing the nitrogen (N) cycle of arable cropping systems is one of the most relevant advantages of cover crops under European conditions. By storing N in the above- and below-ground biomass over winter months, cover crops prevent N leaching losses [1,5–8]. A recent meta-analysis estimated a global reduction in N leaching by 69 % across all species compared to fallow [3]. After termination, N from cover crop biomass might be supplied to succeeding spring cash crops, i.e., maize. The amount of additional N supply to subsequent crops strongly depends on the total N amount, the chemical composition (C/N ratio), and on the duration of decomposition and the resulting mineralisation/immobilisation of N [5]. For cover crop residues with wide C/N ratios, the subsequent N supply can be delayed or reduced [8,9]. Recently, cover crops cultivated as mixtures have received wider recognition in order to provide more diversity in agricultural land and to combine different functional traits in a beneficial way [10,11].

The application of remote sensing techniques in agricultural science and practice is becoming increasingly important. The monitoring of canopy characteristics such as the green area index (GAI), N uptake, or dry matter (DM) accumulation during the vegetation period

is of major interest to understand physiological processes and to further derive management decisions. Many approaches have been developed for yield prediction, phenotyping, and land use monitoring, or to estimate further derived ecosystem services [12–15]. Spectral data are either provided by earth-orbiting satellites such as Landsat or Sentinel [16] or can be assessed with multispectral or hyperspectral sensors from handheld devices [17,18] or mounted on an unmanned airborne vehicle (UAV) [15]. The reflectance behaviour of cash crops, such as maize, soybean, or wheat, has been well studied over the past decades, e.g., by Gitelson et al. [17,19,20] and Bukowiecki et al. [15]. However, few authors have studied cover crops using satellite imagery to determine the current growing area and biomass accumulation of cover crops on a large scale [21,22]. Hively et al. [14] evaluated the N uptake of cover crops, combining on-field destructive plant sampling with hyperspectral measurements and satellite image analysis. Prabhakara et al. [23] found a linear relationship between the normalised difference vegetation index (ND_{red}, commonly known as NDVI) and percent groundcover of six winter cover crop species at the east coast of the United States using a handheld multispectral radiometer. However, so far, no study to our knowledge has estimated the canopy parameters of cover crops on a higher resolution using UAV-based multispectral sensors.

The GAI is a canopy parameter that is directly correlated with the chlorophyll amount and, consequently, can be derived through the spectral reflectance of specific wavelengths. Successful estimates of GAI through remote sensing techniques have been achieved, for example, by Kira et al. [24] for maize and soybean crops using hyperspectral data and by Bukowiecki et al. [15] for wheat with UAV-based multispectral data. Further parameters such as DM and N uptake are regarded as "secondary variables" by Weiss et al. [12]. Compared to the "primary variable" GAI or fraction of photosynthetically active radiation (FPAR), these are not directly correlated to spectral reflectance. Weiss et al. [12] recommended the estimation of "secondary variables" based on knowledge about the physiological dynamics in relation to "primary variables". However, other authors have estimated additional "secondary" canopy parameters empirically, as well. For example, Tucker et al. [18] achieved an R^2 of 0.86 after deriving the biomass of winter wheat directly from spectral reflectance data using a handheld radiometer.

Canopy reflectance within the spectrum of visual light is the response of the chlorophyll content of leaves. More precisely, green light is reflected by the leaves while red light is absorbed by the chloroplasts used for photosynthesis, and is therefore informative about the chlorophyll abundance of the canopy [25,26]. Within near infrared (NIR) wavelengths, reflection reaches higher ranges and delivers structural information about the canopy (leaf angle, thickness, canopy architecture) [24,27]. Another interesting area of wavelengths within the photosynthetic spectrum is the red edge (RE) band, which records the maximum slope in the reflectance spectra and is sensitive to the chlorophyll content of a plant [20,28]. A widespread approach used to combine these informative bands and further increase the contrast in the reflection in NIR and the absorption in red is the computation of a vegetation index (VI) [29]. The most common indices are the normalised difference vegetation index (ND_{red}, commonly known as NDVI [30]) and the simple ratio [31] that is based on red light and NIR reflection. Both VIs can be modified by replacing the red light reflectance with the reflection at RE to increase precision [24,27].

Different canopies show variable reflectance behaviour; hence, the estimations produced by species–individual models tend to be more precise than universal models [27]. Another challenging aspect is the common strategy used to cultivate cover crops as the mixtures of several species for increasing environmental services in an agricultural system [32]. Due to the expected heterogenous spectral response from different species as well as from different mixtures, a comprehensive comparison of universal and individual models seems necessary for winter cover crops. Another challenge is the season in which cover crops are grown. Due to flat sun angles, radiation incidence is reduced in the late autumn and winter months, especially in higher latitudes [33].

The objective of this study was the calibration of the multispectral sensor Sequoia (Parrot) for the canopy parameters of pure stands and mixtures of winter cover crops grown in Northern Germany. Therefore, four different VIs (SR_{red}, $SR_{red\ edge}$, ND_{red}, $ND_{red\ edge}$) were tested for the best regression with each cover crop's GAI, DM, and N uptake, either as a universal or as a species–individual and mixture–individual approach.

2. Materials and Methods

2.1. Study Site

The study site was located in Northern Germany at the Hohenschulen experimental farm of the Kiel University (10.0 E, 54.3 M, 30 m a.s.l.). Glacial influence led to the small scale heterogeneity of soil types. Main soil type is defined as Luvisol with a sandy loam texture in the topsoil. The temperate oceanic climate in the study area is characterised by a long-term average (1991–2020) mean annual air temperature of 9.3 °C and an annual mean precipitation of 797 mm [34].

2.2. Trial Designs

Data collection was carried out in two trials (A and B) in 2018 and 2019 with winter cover crops from different functional groups (Table 1). From trial A, we used 16 randomised plots with four sole cover crops grown after winter oilseed rape. All cover crop treatments in trial A were unfertilized. Trial B was performed in 32 strips with four cover crops as sole stands and four cover crop mixtures. Variations in biomass growth were achieved by implementing two sowing dates and two different nitrogen levels (with and without N fertilisation, N-level adapted according to sowing date, Table 2). Cover crop mixtures sown in Trial B were all possible combinations of the non-winter-hardy species: OR–SO (oilseed radish, saia oats), OR–SV (oilseed radish, spring vetch), SO–SV (saia oat, spring vetch), and OR–SO–SV (oilseed radish, saia oat, common vetch) (Table 1). Winter-hardy rye was not included in the mixture combinations.

Table 1. Winter cover crops investigated in this study.

Cover Crop	Oilseed Radish	Saia Oat	Spring Vetch	Winter Rye
Botanical name	*Raphanus sativus*	*Avena strigosa*	*Vicia sativa*	*Secale cereale*
Family	Brassicaceae	Poaceae	Leguminosae	Poaceae
Abbreviation	OR	SO	SV	WR
Winterhardiness	no	no	no	yes

Table 2. Trial design, sowing dates, and N-level in Trials A and B.

Trial	Sowing Date	Nitrogen Levels (kg N ha^{-1})
Trial A	20 August 2018 23 August 2019	0 (0N)
Trial B	17 August 2018 3 September 2018 24 August 2019 10 September 2019	0 (0N); 60 (60N) 0 (0N); 40 (40N) 0 (0N); 60 (60N) 0 (0N); 40 (40N)

2.3. Reflectance Measurements

Spectral data were collected biweekly with the multispectral camera Sequoia (Parrot), which was mounted to the eBee-X or eBee-SQ drone. The Sequoia (Parrot) camera comprises four spectral bands covering the wavelength ranges of green (550 nm) and red light (660 nm), red edge (RE, 735 nm), and near infrared (NIR, 790 nm). The reflection bands have a bandwidth of 40 nm, except for RE, with 10 nm. Radiometric calibration was performed using a grey scale target, photographed by the camera before each flight. A light

sensor on top of the Sequoia (Parrot) camera measured the incoming radiation. Especially considering the poorer light conditions that occur during the autumn and winter seasons, the values for incoming radiation data became more important for corrections during postprocessing. Flight routes were planned with the software eMotion3 from senseFly. Pixel size was set as 8 cm × 8 cm pixel^{-1}. After each flight, the images recorded with the Sequoia sensor were processed with eMotion3 and Pix4Dmapper software (Pix4D SA., Switzerland). Using Pix4Dmapper, recorded images were processed to orthogonal reflection maps for each reflectance band. Recording an additional image after sampling provided the location and area of the harvested biomass in each plot. The reflectance of the regarded sampling areas was extracted using QGIS (version 3.22.7) and R 4.0.4 [35,36]. To avoid bias due to pixels containing soil or shadow, the median of the extracted pixels served as a representative value [15].

2.4. Plant Sampling

Within two days after each UAV's flight, destructive plant samplings were made. The parameters green area index (GAI, cm^2 cm^{-2}), dry matter (DM, g m^{-2}), and N concentration of DM (%) were determined. Therefore, in each plot, 0.5 m^2 plant material was dug out of the soil. Roots were cut of afterwards to ensure that the complete above-ground biomass was included in the sample. Remaining biomass was fractionated in the green plant material of cover crops, weeds, and senescent plant material. Weeds were dominated by the plants of voluntary oilseed rape. Senescent material was defined as yellow or brown biomass, which was not photosynthetically active. GAI of the green vegetation (cover crop and weed fraction) was measured using the LI-3100C Area Meter (LI-COR Inc., Lincoln, NE USA). The sampled biomass of all fractions was oven-dried at 60 °C for five days and weighted subsequently. N concentration of all fractions was assessed with a CN-Analyser (TruMac CN, LECO) and converted to N uptake g m^{-2} of the regarded DM.

2.5. Statistical Analysis

All calculations were performed in R (Version 4.0.4, R Core Team, 2021). For canopy parameter prediction, simple ratios (SRs) and normalised difference indices (NDs) were calculated, combining the spectral bands red and NIR according to Table 3.

Table 3. Description of vegetation indices investigated in this study with spectral bands used for calculation (NIR: near infrared, RE: red edge, red: red).

Vegetation Index	Abbreviation	Formula	Reference
Simple ratio	SR_{red}	$\frac{NIR}{red}$	Jordan [31]
Simple ratio red edge	$SR_{red\ edge}$	$\frac{NIR}{RE}$	Sims and Gamon [37]
Normalised difference vegetation index	ND_{red}	$\frac{NIR - red}{NIR + red}$	Rouse et al. [30]
Red edge normalised difference vegetation index	$ND_{red\ edge}$	$\frac{NIR - RE}{NIR + RE}$	Dong et al. [38], Gitelson and Merzlyak [39]
Red: 660 nm; RE: 735 nm; NIR: 790 nm			

After selecting the most suitable VI, different model approaches were compared (Figure 1). Measured input data for the canopy parameters referred to the green vegetation. Senescent biomass was excluded, as it showed a low spectral response [23]. One approach was the estimation of the cover crop canopy parameters using a universal model (n = 248). Therefore, the best performing vegetation index was correlated with the measured canopy parameters (GAI, DM, N) across all cover crop species. Furthermore, models were generated for each cover crop separately, and were referred to as species–individual models (n = 65 (OR), n = 53 (SO), n = 65 (SV), n = 65 (WR)).

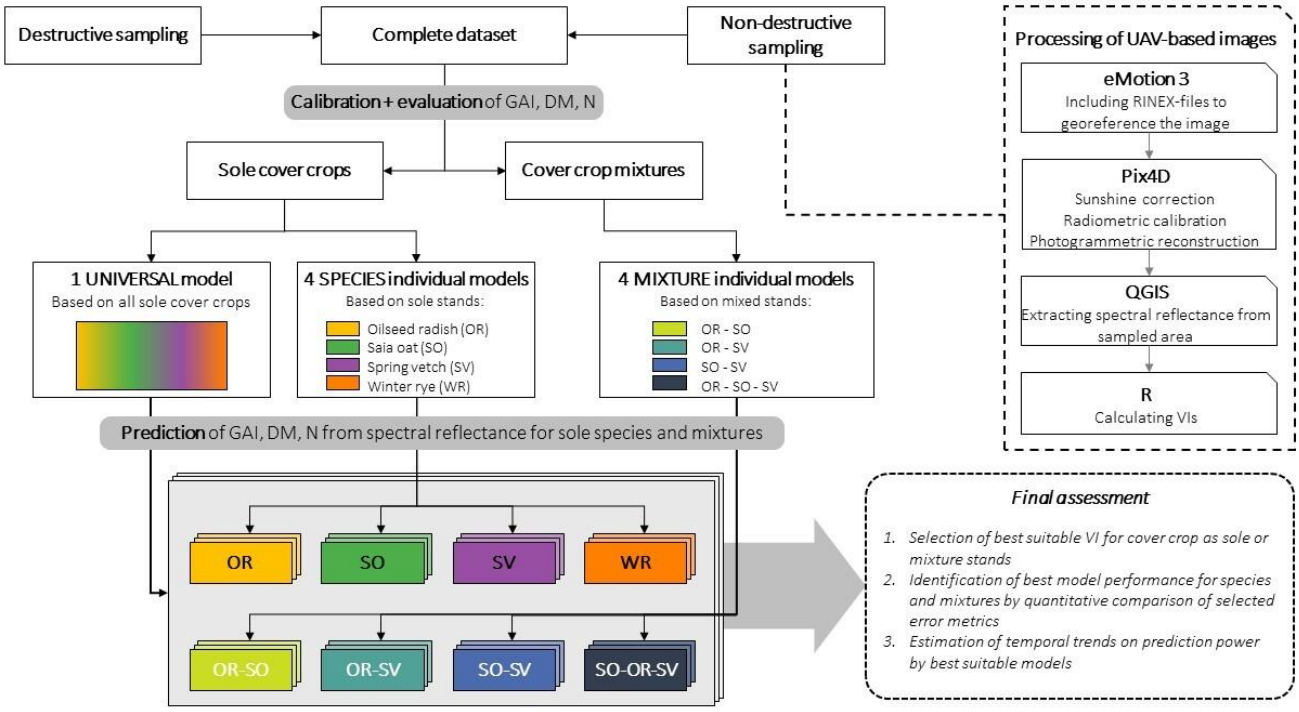

Figure 1. Workflow of the drone-based, non-destructive sampling, model calibrations (universal, species–and mixture–individual model), and the prediction possibilities of the green area index (GAI), dry matter (DM), and N uptake (N) of the respected species or mixture.

For mixed stands, the two model approaches were tested as well. The first assumption was the calibration of the mixture models similar to the species–individual calibration, referred to as the mixture–combination model. Secondly, the universal model based on the sole cover crops was applied to the mixture data set. The data set for cover crop mixtures was restricted to DM and N uptake in 2018 (n = 27 for each cover crop mixture). Relative mean absolute error (rMAE) and adjusted r^2 (R^2) were used to assess error of prediction and for a performance comparison of the VI models.

3. Results

3.1. Weather Conditions

Measured temperature during the observation period ranged from 30 to −1.1 °C in 2018 and 32.1 to −1.3°C in 2019. Frost events (<0 °C) were documented at 28 November 2018 (−1.1 °C), 31 October 2019 (−1.3 °C), and 1 November 2019 (−0.1 °C). Cumulative PAR saturated towards winter in both years and reached a sum of 402.9 W m^{-2} in 2018 and 332.7 W m^{-2} in 2019 (Figure 2).

3.2. Cover Crop DM Accumulation

Crop growth within the plots turned out to be heterogenous. Biomass varied strongly with each sampling date. After the frost events, GAI, DM, and N uptake decreased or saturated. In 2019, frost events occurred earlier in the season, reducing living biomass even more clearly, especially for SV. The data for cover crop mixtures were restricted to DM g m^{-2} and N uptake g m^{-2} in 2018 (Figure 3).

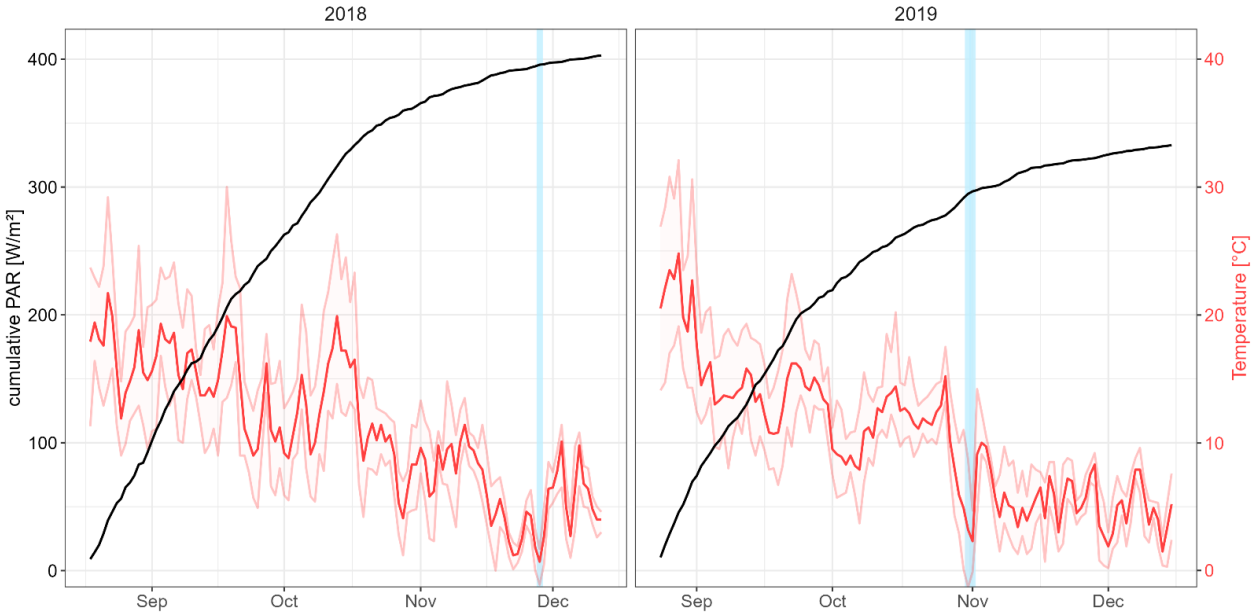

Figure 2. Cumulative photosynthetic active radiation (PAR) (W m^{-2}) (black) and averaged temperature (°C) per day (red) during vegetation periods in 2018 and 2019. The light-red area presents the range according to minimal and maximal temperature (°C) per day. Frost events are illustrated by a blue vertical line (28 November 2018, 31 October 2019, 1 November 2019).

Senescent biomass increased towards the winter month. The highest proportion occurred in winter rye (WR) with 45.7% after a frost event in November 2018. In general, the proportion of senescent plant material was <20% in 2018 and <10%, with the slightly higher values forOR, in 2019. SV showed little to no proportions of senescence for both years (Figure 4).

3.3. Universal Calibration

Linear models were established to predict the parameters GAI, DM, and N uptake of all sole cover crops together by four VIs (SR_{red}, $SR_{red\ edge}$, ND_{red} and $ND_{red\ edge}$). Regarding rMAE and R^2, the universal calibration using SR_{red} to predict GAI performed best (Figure 5). Furthermore, SR_{red} estimated DM and N uptake more precisely than the other VIs (Table 4). ND_{red} models assessed a moderate error but were saturated for GAI values >2 (Figure 5). This also applied for DM g m^{-2} and N uptake g m^{-2} (Table 4). Within lower GAI ranges, the ND_{red} estimated negative values (Figure 5). VIs using the RE band, such as $ND_{red\ edge}$ and $SR_{red\ edge}$, showed higher rMAE compared to their red-based counterparts. The performance of RE-based VIs was almost similar for all regarded canopy parameters (Table 4). Towards a later time of the year, the values of rMAE increased while R^2 decreased (Figure 6), indicating less reliability. Coincidently, a proportion of the senescent biomass increased during the vegetation period (Figure 4). Winter rye reached the highest amount of senescent biomass in December.

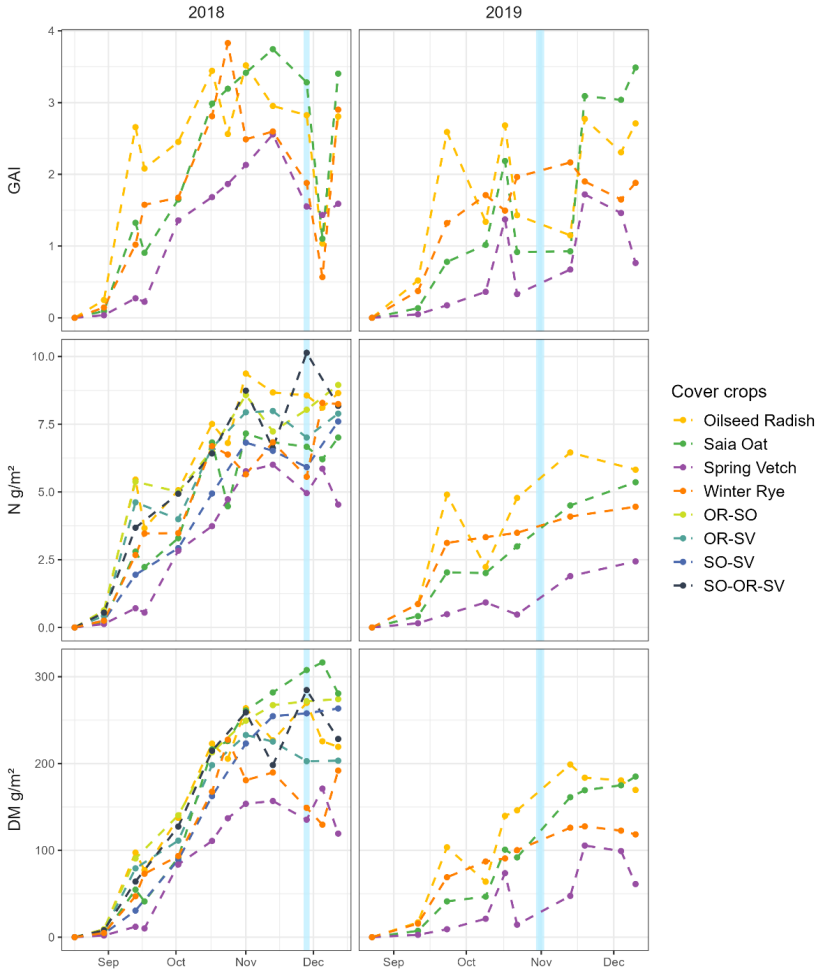

Figure 3. Biomass establishment of sole cover crops and mixtures (OR: oilseed radish, SO: saia oat, SV: spring vetch) presented by green area index (GAI), N uptake (g m^{-2}), and dry matter (DM) (g m^{-2}). Blue vertical lines highlight frost events (28 November 2018, 31 October 2019, 1 November 2019). Point: sampling date; dashed line: linear interpolation between sampling dates.

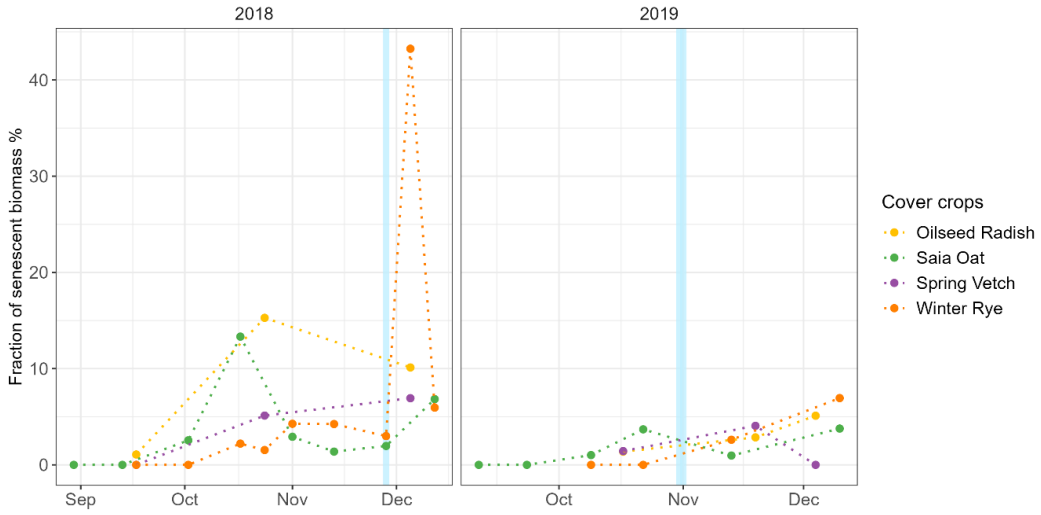

Figure 4. Fraction of senescent biomass (%) in total sampled biomass during the vegetation periods of cover crops in 2018 and 2019. Blue vertical lines highlight frost events (28 November 2018, 31 October 2019, 1 November 2019).

Table 4. Universal models for predicting canopy parameters (green area index (GAI), dry matter (DM) (g m^{-2}), and N uptake (N) (g m^{-2})) of cover crops. For each parameter, four vegetation indices (VIs) (SR_{red}, $SR_{red\ edge}$, ND_{red}, $ND_{red\ edge}$) were tested.

Parameter	VI	Equation	rMAE	R^2
GAI	SR_{red}	−0.21 + 0.19x	31.34	0.60
	$SR_{red\ edge}$	−4.46 + 4.75x	41.46	0.39
	ND_{red}	−2.46 + 5.51x	39.91	0.43
	$ND_{red\ edge}$	−0.05 + 13.74x	40.93	0.40
DM	SR_{red}	−18.51 + 14.56x	50.37	0.53
	$SR_{red\ edge}$	−361.79 + 377.76x	63.38	0.36
	ND_{red}	−204.94 + 441.53x	61.81	0.41
	$ND_{red\ edge}$	−10.66 + 1097.02x	62.67	0.37
N	SR_{red}	0.43 + 0.4x	35.88	0.45
	$SR_{red\ edge}$	−8.1 + 9.72x	43.83	0.26
	ND_{red}	−5.72 + 13.6x	38.91	0.43
	$ND_{red\ edge}$	0.88 + 28.68x	43.37	0.27

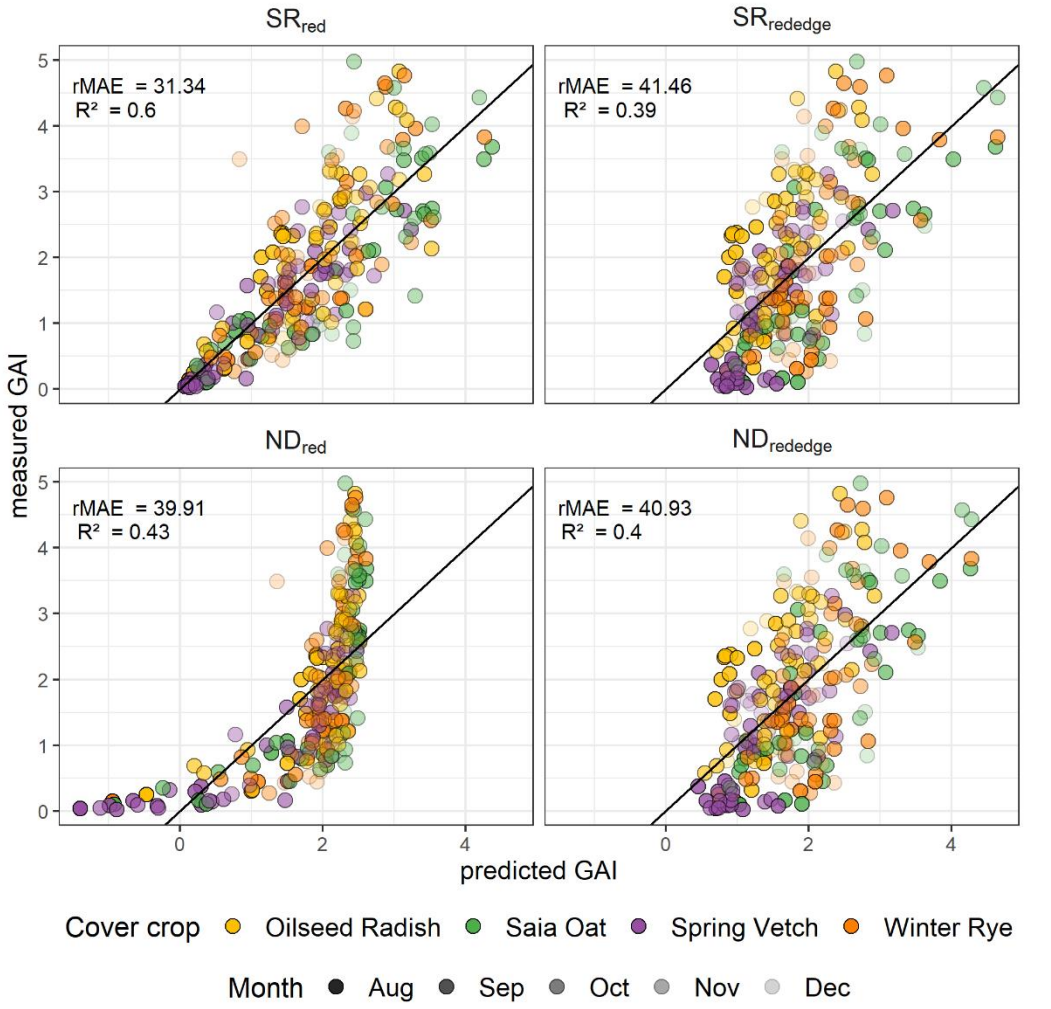

Figure 5. Universal models differing in vegetation indices (simple ratio (SR_{red}, $SR_{red\ edge}$,) and normalised difference vegetation indices (ND_{red}, $ND_{red\ edge}$) for the estimation of the green area index (GAI). Model performance was assessed with relative mean absolute error (rMAE) (%) and R^2.

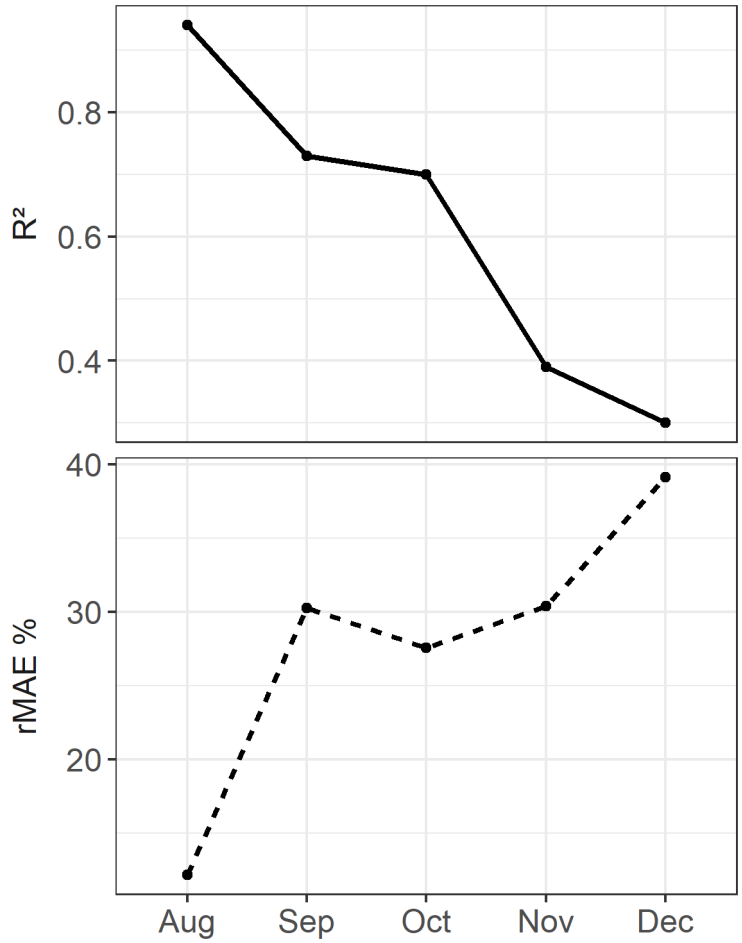

Figure 6. Values of R^2 and relative mean absolute error (rMAE) (%) of the universal SR_{red} model predicting green area index (GAI) over a growth period of cover crops.

3.4. Species–Individual Calibration

For each individual cover crop, the linear models for all regarded canopy parameters with the generically best performing VI SR_{red} were established. In general, the best results of the species–individual models were achieved for the GAI prediction, with an R^2 of 0.76, 0.62, 0.56, and 0.50 for SV, SO, OR, and WR, respectively (Figure 6). The lowest rMAE (25.87%) was calculated for the GAI prediction of SV. The predictions for DM and N uptake were less accurate than GAI (Figure 7). The calibration of SV outperformed the other species with a low average rMAE of 3.68 % and a higher R^2 of 0.22 for all canopy parameters. The lowest accuracy was found for the prediction related to WR across all canopy parameters. Comparing species–individual with the universal model outputs by rMAE, the predictions for all cover crops except for WR were better when using the species–individual models (Figure 8, Table 5). With minor differences, WR's DM and N uptake was somewhat predicted by the universal model. In general, the differences in rMAE for GAI prediction were small (OR: 1.49%; SO: 2.50%; SV: 2.63%; WR: −0.63%). A comparison of the DM prediction resulted in larger differences in favour of the species–individual models, especially for SV and WR (32.93% and 14.45%, respectively).

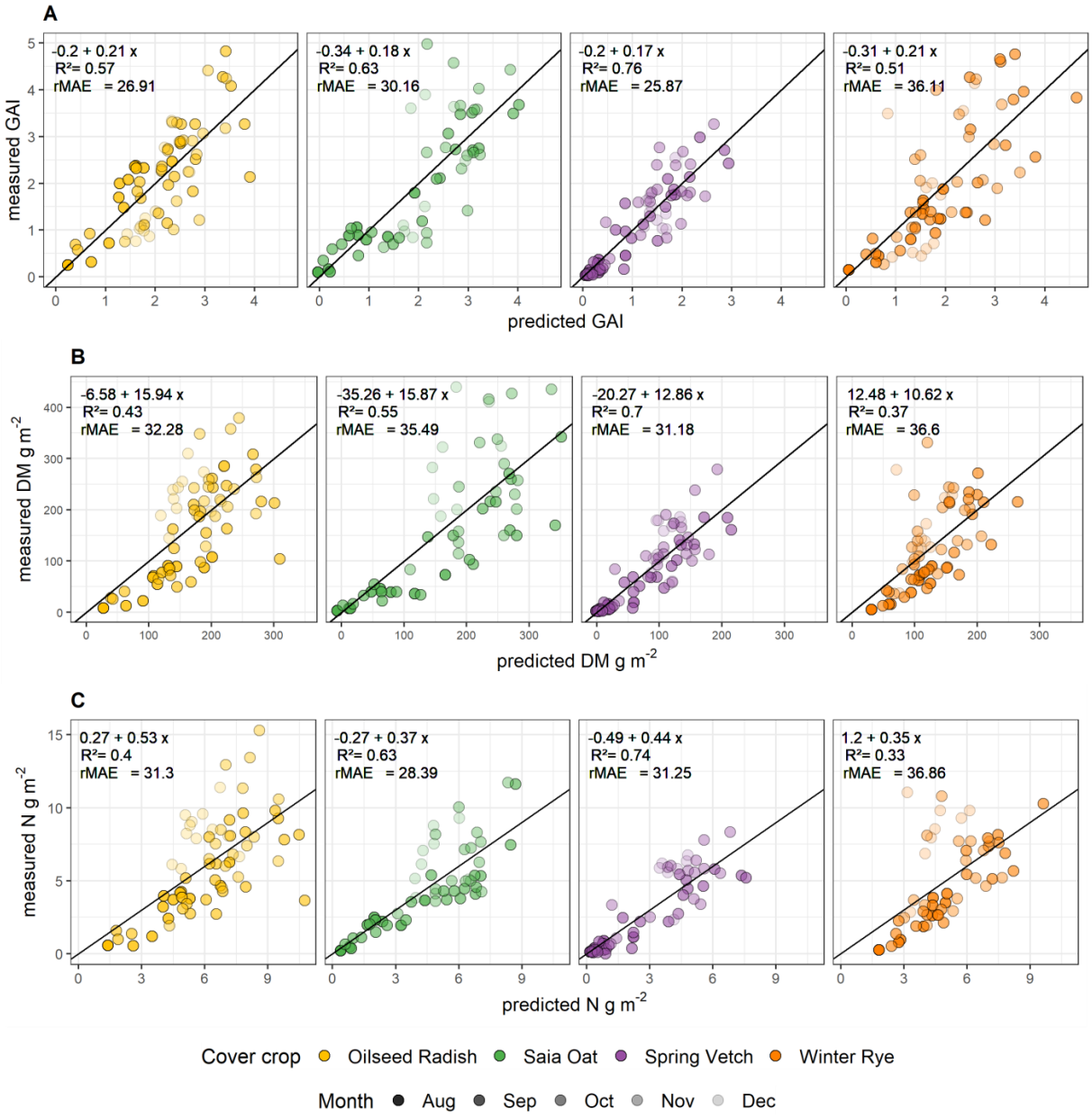

Figure 7. Species-individual models using SR_{red} for estimation of (**A**) green area index (GAI), (**B**) dry matter (DM) (g m^{-2}), and (**C**) N uptake (g m^{-2}). Model performance was assessed with R^2 and the relative mean absolute error (rMAE) (%). Calibration formula is noted for each species and each canopy parameter.

Table 5. Comparison of the two model approaches' prediction performance (species–individual vs. universal models) for green area index (GAI), dry matter (DM), and N uptake (N) by relative mean absolute error (rMAE) (%) for each separate cover crop (oilseed radish, saia oat, spring vetch, winter rye).

Parameter	Species	rMAE %	
		Species–Individual	Universal
GAI	Oilseed Radish	26.91	28.4
	Saia Oat	30.16	32.66
	Spring Vetch	25.87	28.5
	Winter Rye	36.11	35.48

Table 5. *Cont.*

Parameter	Species	rMAE % Species–Individual	rMAE % Universal
DM	Oilseed Radish	32.28	33.26
	Saia Oat	35.49	45.18
	Spring Vetch	31.18	64.11
	Winter Rye	36.6	51.05
N	Oilseed Radish	31.3	33.79
	Saia Oat	28.39	38.27
	Spring Vetch	31.25	39.1
	Winter Rye	36.86	34.47

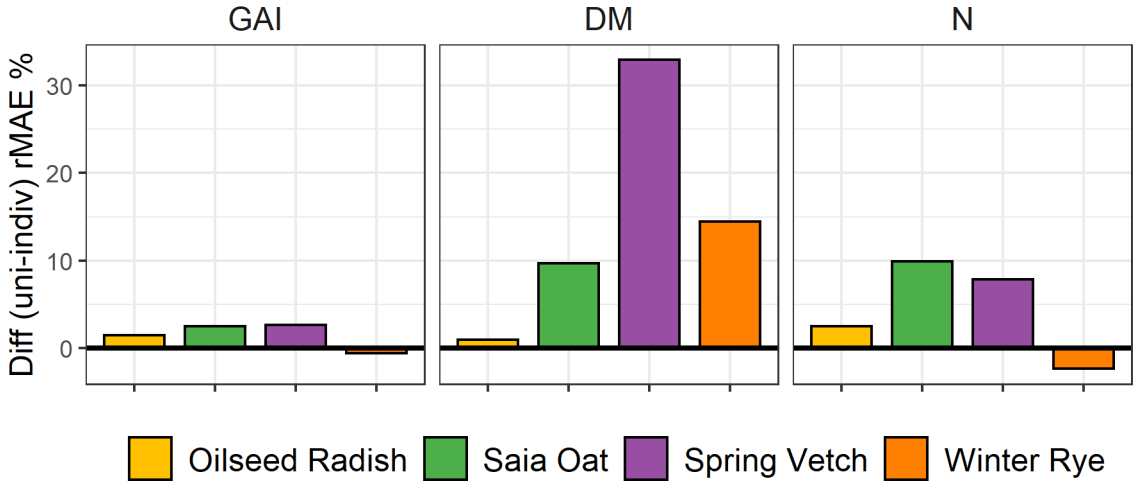

Figure 8. Comparison of the two model approaches' prediction performance for green area index (GAI), dry matter (DM), and N uptake (N) by relative mean absolute error (rMAE) (%). Illustrated is the difference (Diff) of the universal model (uni) calibrated with the sole cover crop data set and the species–individual models (indiv) of each separate cover crop (oilseed radish, saia oat, spring vetch, winter rye).

3.5. Mixture Calibration

In order to predict the N uptake g m^{-2} of cover crop mixtures, two model approaches were compared. The mixture–individual model was related to the spectral reflectance of each cover crop mixtures (Figure 1). The second approach was the estimation made by the universal model, generated with the sole cover crops (OR, SO, WR, SV) based on SR_{red} (Figure 1, Tables 1 and 4). As shown in Figure 9, both the mixture–individual and universal models did not differ in their performance of estimating DM g m^{-2} and N uptake g m^{-2} for mixtures, with relative error differences below 3%. The DM g m^{-2} of OR–SO and SO–SV were rather preferably predicted with the mixture–individual model due to a higher rMAE of the universal model prediction. The N uptake g m^{-2} estimations for the OR–SV, SO–SV, and SO–OR–SV by mixture–individual models were more precise, while N uptake g m^{-2} for OR–SO was somewhat predicted by the universal model. According to R^2, the best estimation for DM and N was achieved by the three-component mixture (SO–OR–SV), with 0.5 and 0.44, respectively (Table 6).

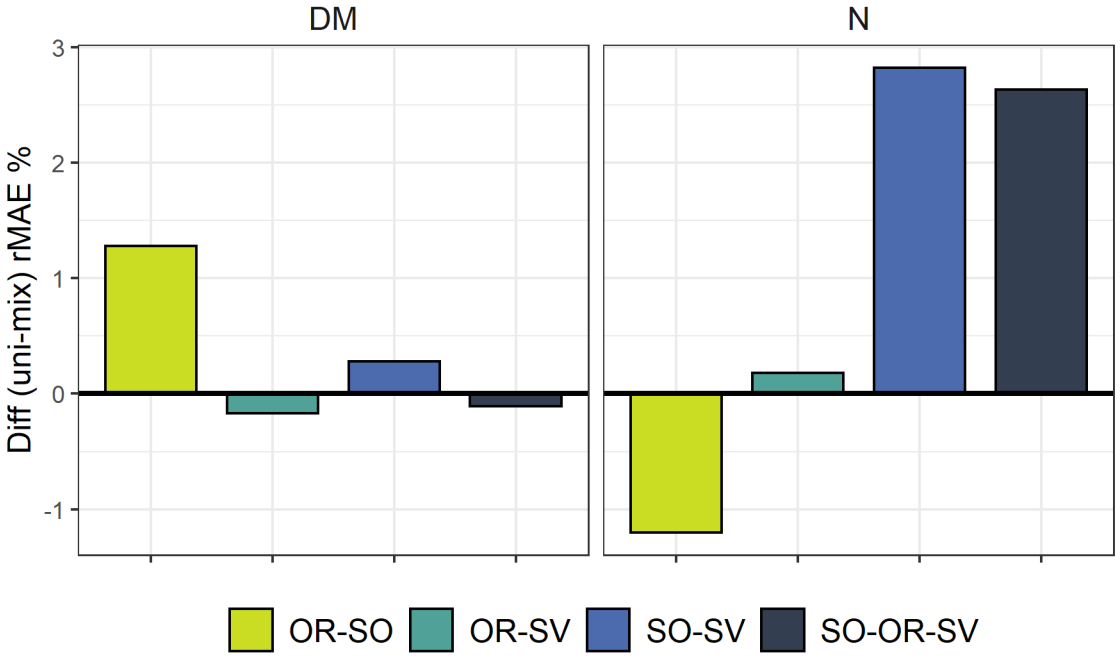

Figure 9. Comparison of the two model approaches' prediction performance for dry matter (DM) and N uptake (N) by relative mean absolute error (rMAE) (%). Illustrated is the difference (Diff) of the universal model (uni) calibrated with the sole cover crop data set and mixture-individual models (mix) of each separate cover crop mixture (OR: oilseed radish, SO: saia oat, SV: spring vetch).

Table 6. Mixture–individual models based on SR_{red} for predicting the canopy parameters (dry matter (DM) (g m^{-2}) and N uptake (N) (g m^{-2})) of cover crop mixtures (OR: oilseed radish, SO: saia oat, SV: spring vetch). Model performance was assessed using the relative mean absolute error (rMAE) (%) and R^2. Calibration formula is noted for each mixture and each canopy parameter.

Parameter	Mixture	Equation	rMAE	R^2
DM	OR–SO	−5.18 + 15.51x	30.71	0.3
	OR–SV	−19.56 + 15.23x	29.18	0.37
	SO–SV	−3.78 + 13.15x	49.04	0.25
	SO–OR–SV	−46.26 + 17.42x	30.3	0.5
N	OR–SO	1.68 + 0.37x	27	0.25
	OR–SV	1.53 + 0.38x	27.18	0.25
	SO–SV	0.58 + 0.32x	33.6	0.35
	SO–OR–SV	0.38 + 0.47x	25.18	0.44

4. Discussion

4.1. Universal Model Approach

Generating universal models based on SR_{red} including all cover crops was the first approach used to estimate GAI, DM g m^{-2}, and N uptake g m^{-2} using the entire data set consisting of 248 measurements for 18 dates. The best results were achieved for the canopy parameter GAI, with an R^2 of 0.60 (Figure 5). GAI directly correlates with the chlorophyll amount in the leaves and thus with the spectral reflectance. The estimations of DM g m^{-2} and N uptake g m^{-2} were less accurate, with an R^2 up to 0.53 and 0.45, respectively (Figure 5). Canopy features such as N uptake or DM do not directly correlate to spectral reflectance, as with GAI [12]; however, species-specific correlations between GAI and these secondary traits indirectly lead to a more or less close correlation to VIs. The prediction power for the "secondary variables" [12] is lower than for GAI; however, modelling the physiological dynamics was, in our study, not superior to the directly estimated ones (data

not shown). However, empirical derivation and thus direct derivation from reflectance data was achieved by several authors for winter wheat. For example, Chen [40] predicted the biomass of with several VIs, reaching a maximal R^2 of 0.86 using NDVI. In addition, Feng et al. [41] found correlations for the leaf N concentration of winter wheat with a large range of VIs. Earlier studies of Tucker et al. [18] showed a good biomass prediction power of the common SR based on NIR and red (R^2: 0.76).

4.2. VI Selection

In this study, two different approaches for the prediction of winter cover crop canopy parameters were examined. The universal and species–individual models of predictions in sole stands based on a simple ratio (SR_{red}) were the most precise compared to the other tested VIs. Typically, implementing the RE band into the VIs' estimations increased the precision due to the strong correlation of chlorophyll content within the RE wavelengths [16,24,28]. Dong et al. [38] compared the performance of conventional VIs, such as SR_{red} and ND_{red}, to RE-based VIs estimating the FPAR of wheat and maize. For both crops, their linear correlations were more stable after implementing RE into the indices. However, in our case, neither the SRs nor NDs performed better when using RE. Considering that most studies observed crop-growing periods during the spring and summer months [15], implementing RE may not be appropriate for the predominant light conditions during the winter season (Figures 2 and 5). Another explanation might be that Sequoia's RE band (10 nm) is narrower than the other bands (40 nm) of the sensor. Due to the heterogenous reflectance of the plants caused by the poor light conditions of autumn and winter, reflectance received in the wavelength of RE in our measurements might be less accurate.

Regarding the most commonly used ND_{red}, the predictions for GAI did not exceed values of 2.6 for canopies with GAIs up to 4.9 (Figure 5). Saturation effects using ND_{red} were also found by Nguy-Robertson et al. [42], predicting the GAI of maize, soybean, wheat, and potato. Modifications of ND_{red} towards the sensitivity of dense stands were partially successful with the wide dynamic range vegetation index (WDRVI), which includes a weighting factor of the vegetative fraction [19,42]. Prabhakara et al. [23] found a linear correlation between ND_{red} and groundcover percentage, studying the reflectance behavior of winter cover crops by using a handheld multispectral radiometer. Groundcover percentage mostly describes the top of the canopy, while GAI, measured in the current study, includes all green areas within the canopy structure of the respected biomass. Specifically, for further derived parameters such as DM accumulation and the N uptake of cover crops, a detailed knowledge of GAI as the primary driver is more important than a rough estimation of the percentage of ground cover which might be sufficient for the estimations of erosion protection potential. In general, ND_{red} is not sensitive to structures beneath the canopy surface, and hence saturates with a higher biomass [43]. Therefore, from the quantitative empirical results as well as from theoretical aspects, the SR based on red band was the preferable VI with which to estimate the functional parameters from the spectral information of winter cover crops.

4.3. Universal vs. Species–Individual and Mixture–Individual Approach

Besides the universal model approach including all cover crops, species–individual models were applied in a second step. Comparing the universal model approach and the species–individual model approach resulted in several differences in favour of the species–individual models, especially for DM and N uptake. GAI estimations showed little differences. SV plots in 2018 were strongly influenced by rapeseed volunteers, which limits the results performed by the SV models in terms of the tested species' characteristics. Corresponding data points were not excluded from the calculations, as a motivation of the study was to reflect the real environmental conditions of winter cover crop cultivation in common cropping sequences. Nevertheless, SV, as a small phenological plant, was easier to calibrate than plants reaching higher values of GAI. The WR–individual model did

not perform better than the universal model for GAI and N uptake (Figure 8), which can be traced back to the high amounts of senescent plant material disturbing the reflectance signal (Figure 4).

Typically, VIs are derived from the reflectance of the wavelength in visible light as well as NIR. The information delivered by NIR reflectance is mostly related to the structural properties of a canopy, such as leaf angle and canopy architecture, while visible light is more related to the activity of absorbers, such as chlorophyll, in the canopy [24,29]. Viña et al. [27] evaluated the performance of multiple VIs for a general correlation in the GAIs of soybean and maize. Except for the RE Chlorophyll Index (CI red edge), all investigated VIs differentiated between both crop types, namely, soybean and maize. The authors cited the differences in chlorophyll distribution within the leaf as the main source for the different depths in the absorption of the red light. Additionally, diverse canopy structures led to a higher reflection in NIR compared to homogenous vegetation coverage [27]. Hence, a sensor calibration for each species individually seems to be most appropriate.

The observed canopies of the winter cover crops were partly mixed with weeds and rapeseed volunteers competing for resources, mainly radiation. The canopy structure was not as homogenous as in a pure wheat or maize canopy, and thus also the spectral reflection. The amount of absorbers and reflectance of radiation differs for each leaf shape and plant type [29]. Consequently, in heterogenous canopies, high precision in a canopy parameter estimation should not be expected.

In cover crop mixtures, the combination of several plants with different characteristics, such as growth behaviour, canopy structure, leaf size, etc., leads to a diverse reflectance throughout the season and within the canopy. Competition between the species makes the emergence and the share of the single crops in the final biomass of a mixed stand unforeseeable, even if it is a well-studied seed mixture. Focussing on cover crops, the composition of a canopy mixture depends on management preferences, soil type, and weather conditions, and is usually independent from the ratio of the sown seeds as the only given measure. As the results showed, sensor calibration for a specific mixture was possible; however, its applicability is questionable (Table 6, Figure 9). A more reliable approach might be to utilize the universal calibration for mixtures with only a slightly reduced performance compared to mixture–individual models.

In general, estimations made using species–individual models achieve more precise results than those made using a universal model. Regarding mixture–individual models, the results did not differ fundamentally. Nevertheless, the universal model approach is based on a larger database than individual models, which makes it more reliable. In addition, the universal model successfully predicted the independent data set of cover crop mixtures.

4.4. Seasonal Challenges

Observing vegetation during autumn and winter using the used Sequoia sensor turned out to be challenging. R^2 decreased to 0.28 in December, while rMAE increased towards 39.12% (Figure 6). The inaccuracy in the winter month can be explained by the low irradiance. PAR saturated in November and December and was even lower in 2019 (Figure 2). Consequently, the sensor receives only a little of the reflectance of the leaves. A second mitigation source is the low sun angle. Assmann et al. [33] found that variation in the sun angle leads to uncertainties in ND_{red} estimates by testing the same Sequoia sensor with several flights in diurnal solar motion in the arctic tundra. At higher latitudes such as Northern Germany, the variation of the sun's angle during a year is up to 40°, resulting in large changes in the incoming radiation. Especially, the growth period of the winter cover crops covers almost the maximum range of the sun's angle. Therefore, the scattering of raw data as well as canopy parameter estimates during winter months might be explainable due to the drastic decline in light incidence. Moreover, our measurements during the respected season were frequently influenced by clouds casting shadows on the study

area, as documented by Assmann et al. [33] in northwestern Canada, by Stow et al. [44] in south–central Scotland, and as reviewed by Aasen et al. [45].

Low temperatures in winter, furthermore, result in an unneglectable and increasing proportion of senescent plant material over time, especially with non-winter-hardy cover crops such as OR, SO, or SV. In the current study, WR—defined as a winter-hardy cover crop—recorded the highest amount of senescent plant material in both years, especially after frost events (Figure 4). Disturbance of the reflectance signal due to senescence was mirrored in the species-individual calibration of WR. The amount of destructive senescent plant material sampled explained a part of the scattering effects in the spectral reflectance. The spectra of the yellow leaves differ from green leaves, as reflection in red and green light increases and decreases in the range of NIR [25,46]. The influence of senescent leaves on the estimates was also shown by Di Bella et al. [47] for ND_{red} in a canopy of Italian ryegrass.

Another source of error is the effect of the saturation of the pixel values. Illumination geometry adjustments have been studied by Olsson et al. [48], who stated that the sunshine sensor of Sequoia (Parrot) is inaccurate if there is a high contrast in the pixel values of the image. Saturation occurs over bright areas such as bare soil, in between and around the observed vegetation, influencing the reflectance and the extracted pixel values. During a few sampling dates, bare soil surrounded the crops or was visible through a sparse stand and led to a noticeable increase in error values (data not shown). Sorting out single images with saturated pixel values even before pre-processing by Pix4D made the reflectance maps more reliable and reduced scattering.

5. Conclusions

The estimation of cover crop canopy parameters can promote the estimation of their effect on the supply of N to cash crops and thereby improve the nitrogen use efficiency of cropping systems. Remote sensing techniques have brought about a huge development in agricultural science and thus to the practice. This study revealed opportunities and challenges for the utilisation of such methods in winter cover crops dealing with vegetative growth periods characterised by the low irradiance and substantial fractions of senescent biomass.

Applying a universal model for winter cover crops seemed to be a sound solution. Species–individual models resulted in somewhat more precise predictions but were based on smaller sub-datasets. Dealing with cover crops involves a huge variation in species and heterogenous canopies compared to cash crops, which are managed as homogenously as possible. SR_{red} was the most sufficient VI tested in this study, irrespective of the model approach used, and was consistently superior to the widely used ND_{red}. In contrast to the often-described advantages of implementing RE instead of red band for the main crops, this did not improve the prediction accuracy in our observed winter cover crops.

Nevertheless, winter cover crops are mostly cultivated for their functional attributes, such as the reduction in nitrate leaching and the improvement of soil properties. Therefore, small inaccuracies in the estimation of GAI, DM g m^{-2}, or N uptake g m^{-2} can be tolerated. The main agronomic focus is to estimate the rough performance of the cultivated winter cover crops in terms of biomass growth and N uptake. Therefore, the findings should serve as a tool for the rapid and inexpensive estimation of the environmental and rotational services of cover crops.

Author Contributions: Conceptualization, K.H. and I.K.; methodology, K.H., T.R. (Thomas Räbiger) and T.R. (Till Rose); software, T.R. (Till Rose); validation, K.H.; formal analysis, I.K.; investigation, K.H. and T.R. (Thomas Räbiger); resources, T.R. (Thomas Räbiger); data curation, K.H.; writing—original draft preparation, K.H.; writing—review and editing, I.K. and H.K.; visualization, K.H.; supervision, I.K.; project administration, T.R. (Thomas Räbiger) and H.K.; funding acquisition, H.K. All authors have read and agreed to the published version of the manuscript.

Funding: This study took place within the joint research project "Reduction of greenhouse gas emissions from crop production through site-specific optimised cover crop systems" (THG ZwiFru),

funded by the German Federal Office for Agriculture and Food on behalf of the Federal Ministry of Food and Agriculture (funding reference no 281B200716).

Data Availability Statement: The code used and the datasets generated during the different steps of the analysis are available from the corresponding author on reasonable request.

Acknowledgments: The authors thank the technical staff Jung, Ziermann, Weise and Schulz for their dedicated field and lab work.

Conflicts of Interest: The authors declare no conflict of interest.

References

1. Abdalla, M.; Hastings, A.; Cheng, K.; Yue, Q.; Chadwick, D.; Espenberg, M.; Truu, J.; Rees, R.M.; Smith, P. A critical review of the impacts of cover crops on nitrogen leaching, net greenhouse gas balance and crop productivity. *Glob. Change Biol.* **2019**, *25*, 2530–2543. [CrossRef] [PubMed]
2. Blanco-Canqui, H.; Mikha, M.M.; Presley, D.R.; Claassen, M.M. Addition of Cover Crops Enhances No-Till Potential for Improving Soil Physical Properties. *Soil Sci. Soc. Am. J.* **2011**, *75*, 1471–1482. [CrossRef]
3. Nouri, A.; Lukas, S.; Singh, S.; Singh, S.; Machado, S. When do cover crops reduce nitrate leaching? A global meta-analysis. *Glob. Change Biol.* **2022**, *28*, 4736–4749. [CrossRef] [PubMed]
4. European Commission. *Report from the Comission to the European Parliament and the Council: On the Implementation of the Ecological Focus Area Obligation under the Green Direct Payment Scheme*; European Commission: Bruessels, Belgium, 2017.
5. Vogeler, I.; Böldt, M.; Taube, F. Mineralisation of catch crop residues and N transfer to the subsequent crop. *Sci. Total Environ.* **2022**, *810*, 152142. [CrossRef]
6. Tonitto, C.; David, M.B.; Drinkwater, L.E. Replacing bare fallows with cover crops in fertilizer-intensive cropping systems: A meta-analysis of crop yield and N dynamics. *Agric. Ecosyst. Environ.* **2006**, *112*, 58–72. [CrossRef]
7. Böldt, M.; Taube, F.; Vogeler, I.; Reinsch, T.; Kluß, C.; Loges, R. Evaluating Different Catch Crop Strategies for Closing the Nitrogen Cycle in Cropping Systems—Field Experiments and Modelling. *Sustainability* **2021**, *13*, 394. [CrossRef]
8. Thorup-Kristensen, K.; Magid, J.; Jensen, L.S. Catch crops and green manures as biological tools in nitrogen management in temperate zones. *Adv. Agron.* **2003**, *79*, 227–302. [CrossRef]
9. Holmes, A.A.; Thompson, A.A.; Lovell, S.T.; Villamil, M.B.; Yannarell, A.C.; Dawson, J.O.; Wortman, S.E. Nitrogen provisioned and recycled by cover crops in monoculture and mixture across two organic farms. *Nutr. Cycl. Agroecosystems* **2019**, *115*, 441–453. [CrossRef]
10. Florence, A.M.; McGuire, A.M. Do diverse cover crop mixtures perform better than monocultures?: A systematic review. *Agron. J.* **2020**, *112*, 3513–3534. [CrossRef]
11. Tosti, G.; Benincasa, P.; Farneselli, M.; Tei, F.; Guiducci, M. Barley–hairy vetch mixture as cover crop for green manuring and the mitigation of N leaching risk. *Eur. J. Agron.* **2014**, *54*, 34–39. [CrossRef]
12. Weiss, M.; Jacob, F.; Duveiller, G. Remote sensing for agricultural applications: A meta-review. *Remote Sens. Environ.* **2020**, *236*, 111402. [CrossRef]
13. Hankerson, B.; Kjaersgaard, J.; Hay, C. Estimation of Evapotranspiration from Fields with and without Cover Crops Using Remote Sensing and in situ Methods. *Remote Sens.* **2012**, *4*, 3796–3812. [CrossRef]
14. Hively, W.D.; Lang, M.; McCarty, G.W.; Keppler, J.; Sadeghi, A.; McConnell, L.L. Using satellite remote sensing to estimate winter cover crop nutrient uptake efficiency. *J. Soil Water Conserv.* **2009**, *64*, 303–313. [CrossRef]
15. Bukowiecki, J.; Rose, T.; Ehlers, R.; Kage, H. High-Throughput Prediction of Whole Season Green Area Index in Winter Wheat with an Airborne Multispectral Sensor. *Front. Plant Sci.* **2019**, *10*, 1798. [CrossRef] [PubMed]
16. Clevers, J.G.P.W.; Gitelson, A.A. Remote estimation of crop and grass chlorophyll and nitrogen content using red-edge bands on Sentinel-2 and -3. *Int. J. Appl. Earth Obs. Geoinf.* **2013**, *23*, 344–351. [CrossRef]
17. Gitelson, A.A.; Viña, A.; Arkebauer, T.J.; Rundquist, D.C.; Keydan, G.; Leavitt, B. Remote estimation of leaf area index and green leaf biomass in maize canopies. *Geophys. Res. Lett.* **2003**, *30*, 1248. [CrossRef]
18. Tucker, C.J.; Holben, B.N.; Elgin, J.H.; McMurtrey, J.E. Remote sensing of total dry-matter accumulation in winter wheat. *Remote Sens. Environ.* **1981**, *11*, 171–189. [CrossRef]
19. Gitelson, A.A. Wide Dynamic Range Vegetation Index for remote quantification of biophysical characteristics of vegetation. *J. Plant Physiol.* **2004**, *161*, 165–173. [CrossRef]
20. Gitelson, A.A.; Viña, A.; Ciganda, V.; Rundquist, D.C.; Arkebauer, T.J. Remote estimation of canopy chlorophyll content in crops. *Geophys. Res. Lett.* **2005**, *32*, L08403. [CrossRef]
21. Hively, W.D.; Duiker, S.; McCarty, G.; Prabhakara, K. Remote sensing to monitor cover crop adoption in southeastern Pennsylvania. *J. Soil Water Conserv.* **2015**, *70*, 340–352. [CrossRef]
22. Goffart, D.; Curnel, Y.; Planchon, V.; Goffart, J.-P.; Defourny, P. Field-scale assessment of Belgian winter cover crops biomass based on Sentinel-2 data. *Eur. J. Agron.* **2021**, *126*, 126278. [CrossRef]

23. Prabhakara, K.; Hively, W.D.; McCarty, G.W. Evaluating the relationship between biomass, percent groundcover and remote sensing indices across six winter cover crop fields in Maryland, United States. *Int. J. Appl. Earth Obs. Geoinf.* **2015**, *39*, 88–102. [CrossRef]
24. Kira, O.; Nguy-Robertson, A.L.; Arkebauer, T.J.; Linker, R.; Gitelson, A.A. Informative spectral bands for remote green LAI estimation in C3 and C4 crops. *Agric. For. Meteorol.* **2016**, *218*, 243–249. [CrossRef]
25. Elvidge, C.D. Visible and near infrared reflectance characteristics of dry plant materials. *Int. J. Remote Sens.* **2007**, *11*, 1775–1795. [CrossRef]
26. Curran, P.J. Remote sensing of foliar chemistry. *Remote Sens. Environ.* **1989**, *30*, 271–278. [CrossRef]
27. Viña, A.; Gitelson, A.A.; Nguy-Robertson, A.L.; Peng, Y. Comparison of different vegetation indices for the remote assessment of green leaf area index of crops. *Remote Sens. Environ.* **2011**, *115*, 3468–3478. [CrossRef]
28. Delegido, J.; Verrelst, J.; Meza, C.M.; Rivera, J.P.; Alonso, L.; Moreno, J. A red-edge spectral index for remote sensing estimation of green LAI over agroecosystems. *Eur. J. Agron.* **2013**, *46*, 42–52. [CrossRef]
29. Myneni, R.B.; Hall, F.G.; Sellers, P.J.; Marshak, A.L. The interpretation of spectral vegetation indexes. *IEEE Trans. Geosci. Remote Sens.* **1995**, *33*, 481–486. [CrossRef]
30. Rouse, J.W.; Haars, J.R.H.; Schell, J.A.; Deering, D.W. Monitoring Vegetation Systemsin the Great Plains Witherts. In Proceedings of the 3rd ERTS Symposium, Washingston, DC, USA, 1 January 1974.
31. Jordan, C.F. Derivation of Leaf-Area Index from Quality of Light on the Forest Floor. *Ecology* **1969**, *50*, 663–666. [CrossRef]
32. Chapagain, T.; Lee, E.A.; Raizada, M.N. The Potential of Multi-Species Mixtures to Diversify Cover Crop Benefits. *Sustainability* **2020**, *12*, 2058. [CrossRef]
33. Assmann, J.J.; Kerby, J.T.; Cunliffe, A.M.; Myers-Smith, I.H. Vegetation monitoring using multispectral sensors—Best practices and lessons learned from high latitudes. *J. Unmanned Veh. Syst.* **2019**, *7*, 54–75. [CrossRef]
34. DWD. Wetter und Klima—Deutscher Wetterdienst: Kiel-Kronshagen (2565). Available online: https://opendata.dwd.de/climate_environment/CDC/observations_germany/climate/multi_annual/mean_91-20/ (accessed on 29 April 2022).
35. R Core Team. *R: A Language and Environment for Statistical Computing*; R Foundation for Statistical Computing: Vienna, Austria, 2021.
36. Hijmans, R.J. *Raster: Geographic Data Analysis and Modeling [R package version 3.5-29]*; Comprehensive R Archive Network (CRAN): Vienna, Austria, 2022.
37. Sims, D.A.; Gamon, J.A. Relationships between leaf pigment content and spectral reflectance across a wide range of species, leaf structures and developmental stages. *Remote Sens. Environ.* **2002**, *81*, 337–354. [CrossRef]
38. Dong, T.; Meng, J.; Shang, J.; Liu, J.; Wu, B. Evaluation of Chlorophyll-Related Vegetation Indices Using Simulated Sentinel-2 Data for Estimation of Crop Fraction of Absorbed Photosynthetically Active Radiation. *IEEE J. Sel. Top. Appl. Earth Obs. Remote Sens.* **2015**, *8*, 4049–4059. [CrossRef]
39. Gitelson, A.A.; Merzlyak, M.N. Signature Analysis of Leaf Reflectance Spectra: Algorithm Development for Remote Sensing of Chlorophyll. *J. Plant Physiol.* **1996**, *148*, 494–500. [CrossRef]
40. Chen, P. A Comparison of Two Approaches for Estimating the Wheat Nitrogen Nutrition Index Using Remote Sensing. *Remote Sens.* **2015**, *7*, 4527–4548. [CrossRef]
41. Feng, W.; Zhang, H.-Y.; Zhang, Y.-S.; Qi, S.-L.; Heng, Y.-R.; Guo, B.-B.; Ma, D.-Y.; Guo, T.-C. Remote detection of canopy leaf nitrogen concentration in winter wheat by using water resistance vegetation indices from in-situ hyperspectral data. *Field Crops Res.* **2016**, *198*, 238–246. [CrossRef]
42. Nguy-Robertson, A.L.; Peng, Y.; Gitelson, A.A.; Arkebauer, T.J.; Pimstein, A.; Herrmann, I.; Karnieli, A.; Rundquist, D.C.; Bonfil, D.J. Estimating green LAI in four crops: Potential of determining optimal spectral bands for a universal algorithm. *Agric. For. Meteorol.* **2014**, *192*, 140–148. [CrossRef]
43. Myneni, R.B.; Williams, D.L. On the relationship between FAPAR and NDVI. *Remote Sens. Environ.* **1994**, *49*, 200–211. [CrossRef]
44. Stow, D.; Nichol, C.; Wade, T.; Assmann, J.; Simpson, G.; Helfter, C. Illumination Geometry and Flying Height Influence Surface Reflectance and NDVI Derived from Multispectral UAS Imagery. *Drones* **2019**, *3*, 55. [CrossRef]
45. Aasen, H.; Honkavaara, E.; Lucieer, A.; Zarco-Tejada, P. Quantitative Remote Sensing at Ultra-High Resolution with UAV Spectroscopy: A Review of Sensor Technology, Measurement Procedures, and Data Correction Workflows. *Remote Sens.* **2018**, *10*, 1091. [CrossRef]
46. Royimani, L.; Mutanga, O.; Dube, T. Progress in Remote Sensing of Grass Senescence: A Review on the Challenges and Opportunities. *IEEE J. Sel. Top. Appl. Earth Obs. Remote Sens.* **2021**, *14*, 7714–7723. [CrossRef]
47. Di Bella, C.M.; Paruelo, J.M.; Becerra, J.E.; Bacour, C.; Baret, F. Effect of senescent leaves on NDVI-based estimates of f APAR: Experimental and modelling evidences. *Int. J. Remote Sens.* **2010**, *25*, 5415–5427. [CrossRef]
48. Olsson, P.-O.; Vivekar, A.; Adler, K.; Garcia Millan, V.E.; Koc, A.; Alamrani, M.; Eklundh, L. Radiometric Correction of Multispectral UAS Images: Evaluating the Accuracy of the Parrot Sequoia Camera and Sunshine Sensor. *Remote Sens.* **2021**, *13*, 577. [CrossRef]